Thermogenic Methane Production in Antarctic Subglacial Hydrocarbon Seeps

Gavin Piccione[1,2*], Jared E. Nirenberg[1,2], Joseph Novak[3], Abigale Hawthorn[4], Paul Northrup[5], Terrence Blackburn[4], Daniel E. Ibarra[1,2]

[1]Department of Earth, Environmental, and Planetary Sciences, Brown University, Providence, RI 02906, USA.
[2]Institute at Brown for Environment and Society, Brown University, Providence, RI 02906, USA.
[3]Ocean Sciences Department, University of California Santa Cruz, Santa Cruz, CA 95064, USA.
[4]Earth and Planetary Sciences, University of California Santa Cruz, Santa Cruz, CA 95064, USA.
5Department of Geosciences, Stony Brook University, Stony Brook, NY 11794, USA.

Corresponding author: Gavin Piccione (gavin_piccione@brown.edu)

This is a non-peer reviewed preprint submitted to EarthArXiv.

This manuscript has submitted for peer review to *Geology*.

ABSTRACT

Methane forms beneath ice sheets through microbial methanogenesis and thermogenic breakdown of organic matter, creating a potentially large greenhouse gas reservoir prone to release during glacial retreat. Subglacial thermogenic methanogenesis can increase gas buildup and create oases for life, but this process has not yet been observed in Antarctica, contributing to uncertainty in the spatial distribution and magnitude of methane reserves beneath the ice sheet. Here, we present evidence of Antarctic subglacial thermogenic methane production in shallow basal sediments, preserved in carbonate nodules collected at Elephant Moraine and the Pensacola Mountains, East Antarctica. Oxygen and uranium-series isotope analyses indicate that these carbonates precipitated from glacial meltwater during deglacial periods in the late Pleistocene. Carbonate $\delta^{13}C$ values as low as -32.75 ‰ identify thermogenic methane as a primary carbon source, while clumped isotope measurements indicate formation temperatures of 12 - 20˚C, consistent with a geothermal origin. Lipid biomarker analyses further show that organic matter preserved in the nodules is highly thermally matured. These findings indicate that deep-sourced thermogenic methane migrated as hydrocarbon seeps to shallow pore spaces within basal sediments, demonstrating that geothermally active areas can be hotspots for methane accumulation below the Antarctic Ice Sheet. High manganese concentrations and the presence of pyrite oxidation products in the carbonate nodules suggest that this methane was oxidized via sulfate or manganese reduction by chemosynthetic microbes. Subglacial hydrocarbon seeps may thus represent habitable environments in isolated subglacial environments on Earth and icy planetary bodies.

INTRODUCTION

The Antarctic Ice Sheet stores vast reservoirs of organic carbon at its bed in the form of legacy soil, vegetation, and sediment overridden during glacial advance (Wadham et al., 2012). Microbes can remineralize this organic matter to CO_2 using available terminal electron acceptors including O_2, introduced from ice melt or bedrock-derived NO_3^-, Fe^{3+} or SO_4^{2-}. In isolated subglacial environments, these higher-energy electron acceptors can be depleted over time, shifting carbon cycling to methanogenesis (Boyd et al., 2010; Stibal et al., 2012). The thermogenic breakdown of legacy organic matter can also generate subglacial methane (Wadham et al., 2012). High pressures and low temperatures at the ice sheet bed can promote the accumulation of methane in sediment porewaters, forming a potentially unstable reservoir of potent greenhouse gases that may be released during glacial retreat (Wadham et al., 2012). Evidence for methane release has been observed in modern proglacial regions of the Greenland Ice Sheet (Dieser et al., 2014; Christiansen and Jørgensen, 2018; Lamarche-Gagnon et al., 2019), and during the last deglaciation (17 -7 ka) of the Scandinavian Ice Sheet (Crémière et al., 2016).

In Antarctica, biologic methane production has been detected in the sediment pore waters of Subglacial Lakes Whillans (Michaud et al., 2017) and Mercer (Davis et al., 2023), but is largely consumed by microbes in the oxygen-rich lake water before it can accumulate. Thermogenic methane production in subglacial environments can lower the oxidative capacity of basal water, creating conditions that enhance microbial methanogenesis and promote methane buildup (Burns et al., 2018). Biogenic and thermogenic methane impart distinct carbon isotope signatures (-110‰ to -50‰ versus -50‰ to -20‰, respectively (Whiticar, 1999)), which can be preserved in carbonate minerals. In other settings, thermogenic methane release is often associated with hydrocarbon seeps and carbonate precipitation, forming habitats that support diverse microbial and macrofaunal communities (Joye, 2020). Similar processes may provide important habitats for life under extreme conditions beneath ice sheets. However, thermogenic methane release has not been

directly observed beneath the Antarctic Ice Sheet, leaving uncertainty in the magnitude of basal methane reserves and the distribution of these potentially important ecosystems. Here, we present evidence for Antarctic subglacial thermogenic methane production, preserved in carbonate nodules collected in surface till at Elephant Moraine and the Pensacola Mountains (Fig. 1). We characterized carbonate parent waters using oxygen isotopes and synchrotron-based microspectroscopy, determined nodule formation timing and temperature with U-series and clumped isotopes, and constrained inorganic and organic carbon sources through carbon isotope and biomarker analyses. Our results indicate that these carbonates formed from a mixture of glacial meltwater that percolated into sediment pore spaces and thermogenic methane that migrated upwards into the shallow sediments as hydrocarbon seeps. Geochemical and mineralogic signatures suggest that some of this methane was oxidized by sulfate or manganese reduction, likely mediated by chemosynthetic organisms. These subglacial carbonates offer unique insights into methane production and carbon cycling in the Antarctic basal environment.

METHODS AND RESULTS

We analyzed carbonate nodules collected from supraglacial moraines in blue ice at Elephant Moraine in the David Glacier Catchment (n=1) and Mount Wanous in the Patuxent Range of the Pensacola Mountains (n = 5) in East Antarctica (Fig. 1). Till in both moraines originates from the ice sheet bed and is exhumed to the surface within basal ice (Faure, 1990; Cassidy et al., 1992).

We integrate $\delta^{13}C$, $\delta^{18}O$, and carbonate clumped isotope analyses with X-Ray Fluorescence (XRF) and X-Ray Absorption Near Edge Spectroscopy (XANES) measurements to characterize the carbonate formation environment and parent water chemistry. Carbonate $\delta^{18}O$ values, range from -47.3‰ to -34.7‰ (VSMOW) (Fig. 2a). These values are presented as water-equivalent $\delta^{18}O$, calculated using the calcite-water fractionation factor from Kim and O'Neil (1997), with temperatures either constrained by carbonate clumped isotope data or set to the average Δ_{47}-derived temperature (17.2˚C) for samples lacking such measurements. Carbonate clumped isotope ratios (Δ_{47}; 0.587 – 0.65) indicate formation temperatures of 12–20˚C (Fig. 2b). XRF maps and microbeam XANES data from a Pensacola carbonate reveal Fe and Mn enrichment. XANES confirms that Mn is a mixture of Mn(II) in the carbonate lattice and Mn(IV) in detrital sediments, while Fe(II) is present as ferrous sulfate (Fig. 3).

Carbon isotope analyses of bulk carbonate and isolated organic matter within the nodules are used to characterize the source of organic and inorganic carbon. Pensacola carbonates exhibit $\delta^{13}C$ values ranging from -30.8 ‰ to -13.2 ‰ (VPDB), whereas the Elephant moraine carbonate has values between -10.3 ‰ and -10.8 ‰ (Fig. 2). The $\delta^{13}C$ of organic matter preserved in the carbonates range from -25.4 to -22.9 ‰ (Fig. 2).

Linear alkane (*n*-alkane) distributions reflect a high degree of thermal maturation. Specifically, the carbon preference index (CPI) of *n*-alkanes – an indicator of petrogenesis – approaches 1 in all samples (Fig. 4), consistent with the composition of petroleum source beds (Bray and Evans, 1961). Likewise, we observe a preference for short chain and mid chain (C_{16} to C_{26}) over long chain (C_{27}-C_{40}) *n*-alkanes in all samples, a pattern characteristic of paraffins recovered from crude oil and petroleum source beds (Bray & Evans, 1961).

U-series analyses were measured to constrain the timing of nodule formation. The Elephant Moraine precipitate has an initial $^{234}U/^{238}U$ activity ratio ($[^{234}U/^{238}U]_i$) of 2.93 and a formation age of 384.27 ka ± 6.43 ka (1σ). Samples from the Pensacola Mountains have high Th concentrations (~7 ppm), necessitating U-Th isochrons for age determination. A U-Th isochron age of 12.6 ka ±

3.4 ka and a $[^{234}U/^{238}U]_i$ of 1.52 was determined for one of the Pensacola nodules (See the Supplementary Materials).

DISCUSSION

The carbonate nodules studied here resemble those found in subsurface sedimentary sequences associated with hydrocarbon seeps in both shape and texture (Little et al., 2015). They preserve fine sedimentary features, including irregular laminations and detrital inclusions, suggesting formation as carbonate cements. They also all have a distinctive dome shape that likely reflects formation at a sediment size or porosity boundary, or in a cavity within the shallow sediment column (Wu et al., 2021).

Carbonates from the Pensacola Mountains have $\delta^{13}C$ values as low as -32.8‰, aligning with the composition of thermogenic methane (-50‰ to -20‰) and exceeding the expected range for microbially-produced methane (-110‰ to -50‰) (Whiticar, 1999). Several carbonates have $\delta^{13}C$ values clustering around -30‰, indicating that thermogenic methane was a dominant source of carbon in these porewaters. The absence of lower $\delta^{13}C$ values indicates minimal microbial methanogenesis. Other carbonate $\delta^{13}C$ values extend up to -10.3‰. suggesting the incorporation of less ^{13}C-depleted carbon (Naehr et al., 2007).

Carbon isotope compositions of organic matter preserved in the carbonate nodules (-25.4 to -22.9 ‰) fall within the range of C_3 terrestrial plant matter (Lamb et al., 2006), while *n*-alkane CPI shows that this organic matter is highly thermally matured, with distributions characteristic of petroleum source beds (Fig. 4). Remineralization of this organic matter could contribute additional carbon to parent waters, which would drive the $\delta^{13}C$ of the carbonates above thermogenic methane compositions. Many of the Pensacola nodules have $\delta^{13}C$ values lower than these organic matter, providing further evidence that dissolution of thermogenic methane was a primary source of carbon. In contrast, carbonates with higher $\delta^{13}C$ values (-20.09 and -10.3 ‰) suggest mixing between methane-derived carbon and a more ^{13}C-enriched source, likely carbonate bedrock or CO_2 from melted glacial ice. Additionally, microbial methanogenesis may have increased $\delta^{13}C$ values of dissolved inorganic carbon (Cochran et al., 2022).

For the Elephant moraine carbonate, the $\delta^{13}C$ alone cannot determine the presence of thermogenic methane. However, most hydrocarbon seeps are methane dominated (Sun et al., 2020), and petroleum biomarkers are often associated with methane release (Kvenvolden and Rogers, 2005). The combined geochemical evidence suggests that this carbonate nodule formed in a subglacial hydrocarbon seep in conditions conducive to methane accumulation.

The carbonate nodules exhibit $\delta^{18}O$ values ranging from -38.6 to -34.7‰ in the Pensacola samples and -47.3 ‰ in the Elephant moraine sample, consistent with parent waters derived from melted glacial ice (Fig. 2). Elevated clumped isotope temperatures (12–20°C) suggest that ice melting was driven by geothermal heating (Fig. 3). Given that the ice sheet in both regions is at least several hundred of meters thick (Fretwell et al., 2013), geothermal heat is unlikely to reach the ice sheet surface. Instead, the geothermally elevated formation temperatures indicate that carbonate nodules formed in the subglacial environment.

Geochemical data from the carbonate nodules support the introduction of deep thermogenic carbon to shallow subglacial porewaters. Anaerobic methane oxidation occurs where sulfate and methane coexist, typically within a few meters of the sediment water interface in shallow terrestrial water bodies (Cochran et al., 2022). The $\delta^{18}O$ values, which match glacial ice, further suggest carbonate formation near the sediment-water interface, where melted ice can fill pore spaces. In contrast deeper seep carbonates typically have higher $\delta^{18}O$ values due to clay dewatering and

methane hydrate destabilization (Cochran et al., 2022). Additionally, mixing of thermogenic methane and less ^{13}C-depleted carbon sources (e.g. organic matter, carbonate, or CO_2 from glacial ice) is more likely near the sediment-water interface, whereas deeper seeps are dominated by methane-derived carbon (Cochran et al., 2022).

The observation of ferrous sulfate within the carbonate nodules – an oxidation product of pyrite commonly found in methane seeps (Huggins et al., 1988; Yang et al., 2021) – suggests that pyrite was originally present in the system. This implies that thermogenic methane was anaerobically oxidized to CO_2 via sulfate reduction (Cochran et al., 2022). The formation temperatures of these nodules (12-20˚C) strongly suggests that this process occurred through microbial activity (Boetius et al., 2000), as thermochemical sulfate reduction requires temperatures >100˚C (Machel, 2001). Additionally, the incorporation of Mn(II) in the carbonate lattice indicates a possible second mechanism for methane dissolution, as Mn was likely concentrated in carbonate parent waters through the reduction of Mn(IV)-bearing detrital minerals–a process that can also be coupled with anerobic methane oxidation by chemosynthetic microorganisms (Beal et al., 2009).

Implications of Antarctic Subglacial Thermogenic Methane

U-series ages from both Elephant Moraine and Pensacola samples indicate that hydrocarbon seep carbonates formed during periods of ice thinning. The Elephant Moraine carbonate dates to 384.27 ka ± 12.85 ka, during Marine Isotope Stage 11 (MIS 11): the warmest Pleistocene interglacial period when ice in this region likely thinned considerably (Blackburn et al., 2020). The Pensacola samples formed at 12.6 ka ± 3.4 ka, coinciding with ice thinning in the Pensacola Mountains during the last deglaciation (Bentley et al., 2017). Ice sheet retreat can destabilize methane reservoirs (Portnov et al., 2016), thus the presence of subglacial hydrocarbon seeps during periods of ice thinning suggests a potential link between Antarctic ice loss and thermogenic methane release, warranting future study.

The formation of carbonate and pyrite, along with elevated manganese concentrations in the studied carbonates, indicates that thermogenic methane is at least partially degraded to CO_2 in the subglacial environment through anerobic oxidation coupled to manganese and sulfate reduction (Paull et al., 1992; Beal et al., 2009), preventing its release to the atmosphere. These microbial processes suggest the presence of chemosynthetic organisms adapted to extreme basal conditions (Boetius et al., 2000; Beal et al., 2009). Such ecosystems are of particular interest because hydrocarbon seeps have been proposed as terrestrial analogs for habitable zones on icy planetary bodies such as Europa, Enceladus, and Titan (Preston and Dartnell, 2014). Antarctica's isolated subglacial environment offers a valuable Earth-based counterpart to these extraterrestrial settings. The hydrocarbon seep carbonates examined here form in areas of moderate geothermal activity in East Antarctica (see the Supplementary Materials), while other sedimentary basins (Aitken et al., 2023) in regions of high geothermal heat flux—particularly along the West Antarctic Rift System—may sustain thermogenic methane production and chemosynthetic ecosystems on a broader scale (Wadham et al., 2012).

CONCLUSIONS

Carbonates collected in supraglacial moraines in the Pensacola Mountains and David Glacier Catchment record thermogenic methane flux in the subglacial environment during the late Pleistocene. Chemical and mineralogic evidence in these samples demonstrates that methane migrates from depth into shallow sedimentary pore spaces, where it is anaerobically oxidized by microbial reactions linked to sulfate and manganese reduction. These results imply that

thermogenic methane production contributes to methane and carbon dioxide reserves beneath the Antarctic Ice Sheet. Subglacial hydrocarbon seeps may sustain ecosystems that support chemosynthetic organisms and are a potential analog for habitable zones on icy planetary bodies.

ACKNOWLEDGEMENTS

We thank John Schutt for collecting the sample from Elephant Moraine, and for useful discussion of the sample collection area. We are grateful to Ryan Tappero who guided synchrotron analyses. This work was supported by NSF Office of Polar programs award numbers 2045611, 2042495, and 2423761 to TB, and support from the Institute at Brown for Environment and Society to DEI. This material is based on services provided by the Polar Rock Repository with support from the National Science Foundation, under Cooperative Agreement OPP-2137467.

FIGURES CAPTIONS

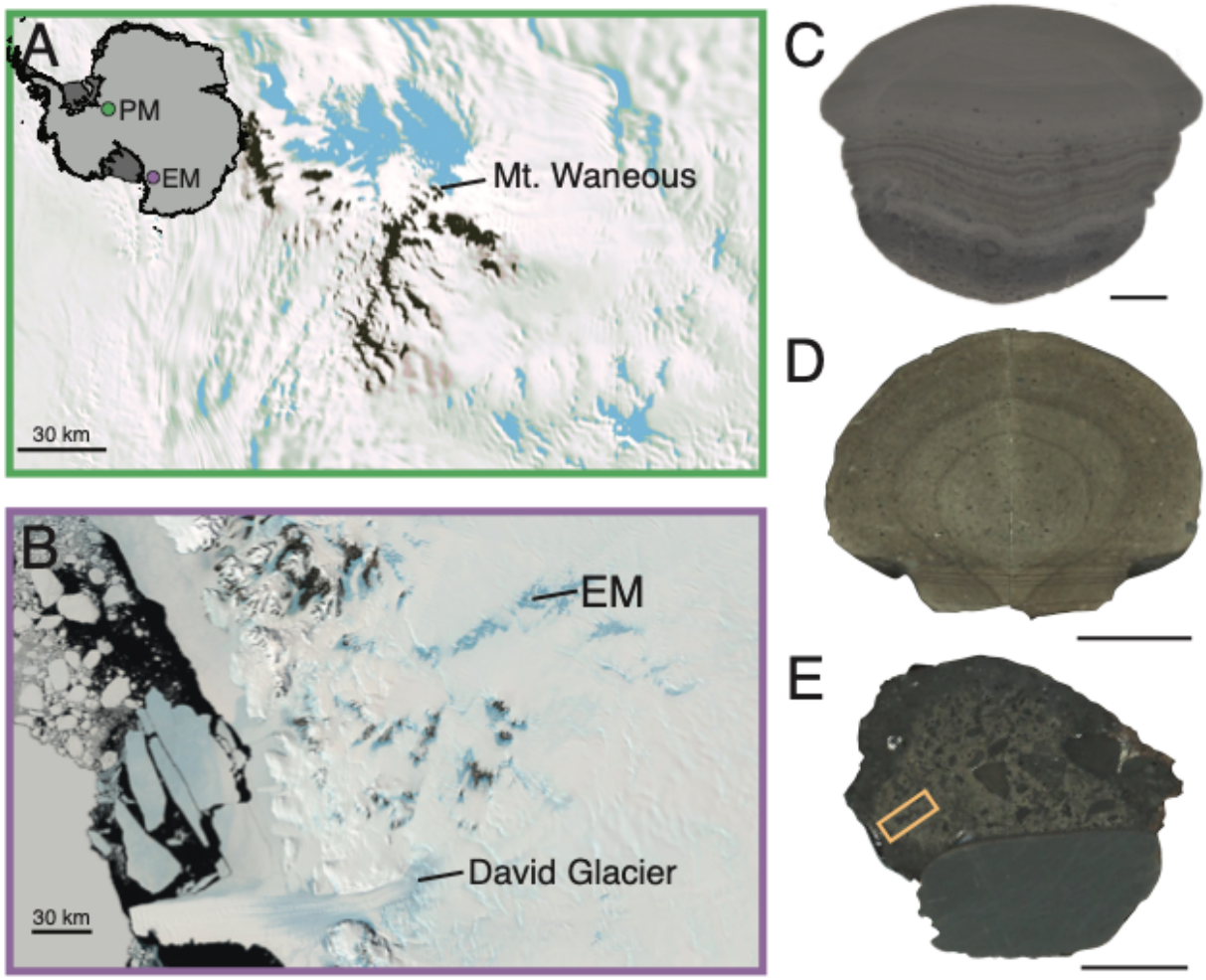

Figure 1. A,B: Satellite images of samples collection locations in the Pensacola Mountains and Elephant Moraine, respectively. C: Carbonate nodule from Elephant Moraine. D,E: Representative examples of carbonate nodules from the Pensacola Mountains. Scale bars are 1cm. Yellow box on bottom represents area analyzed for XRF and XANES.

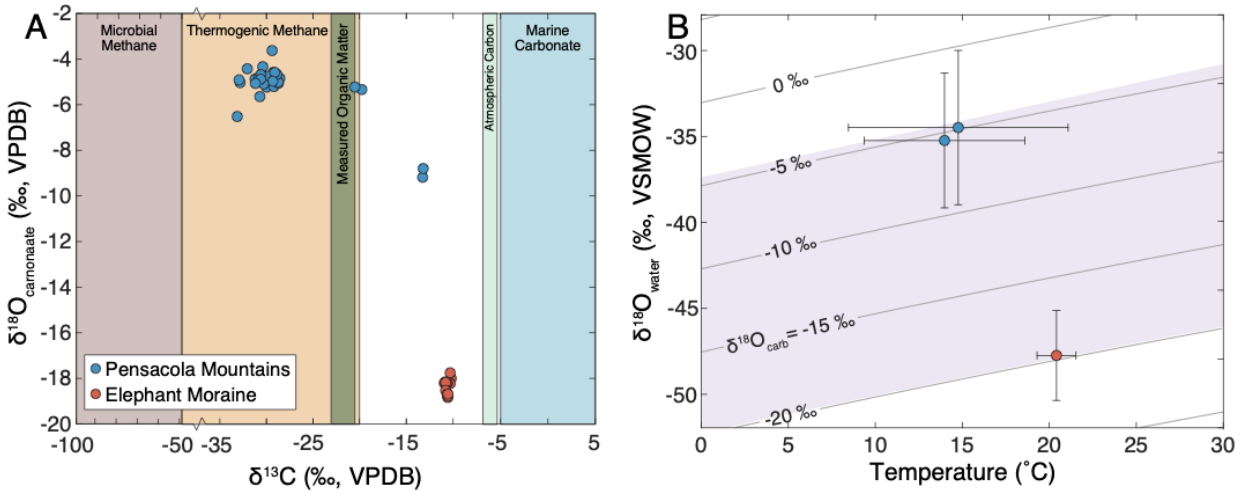

Figure 2: A: Carbonate $\delta^{18}O$ versus $\delta^{13}C$ (‰, VPDB) values. Colored regions represent potential carbon source compositions. B: $\delta^{18}O_{water}$ versus Δ_{47}-derived temperatures. Gray lines represent equilibrium $\delta^{18}O$ of carbonate, calculated from equilibrium calcite-water oxygen isotope fractionation (Kim and O'Neil 1997). Shaded region represents distribution of measured $\delta^{18}O$ carbonate values.

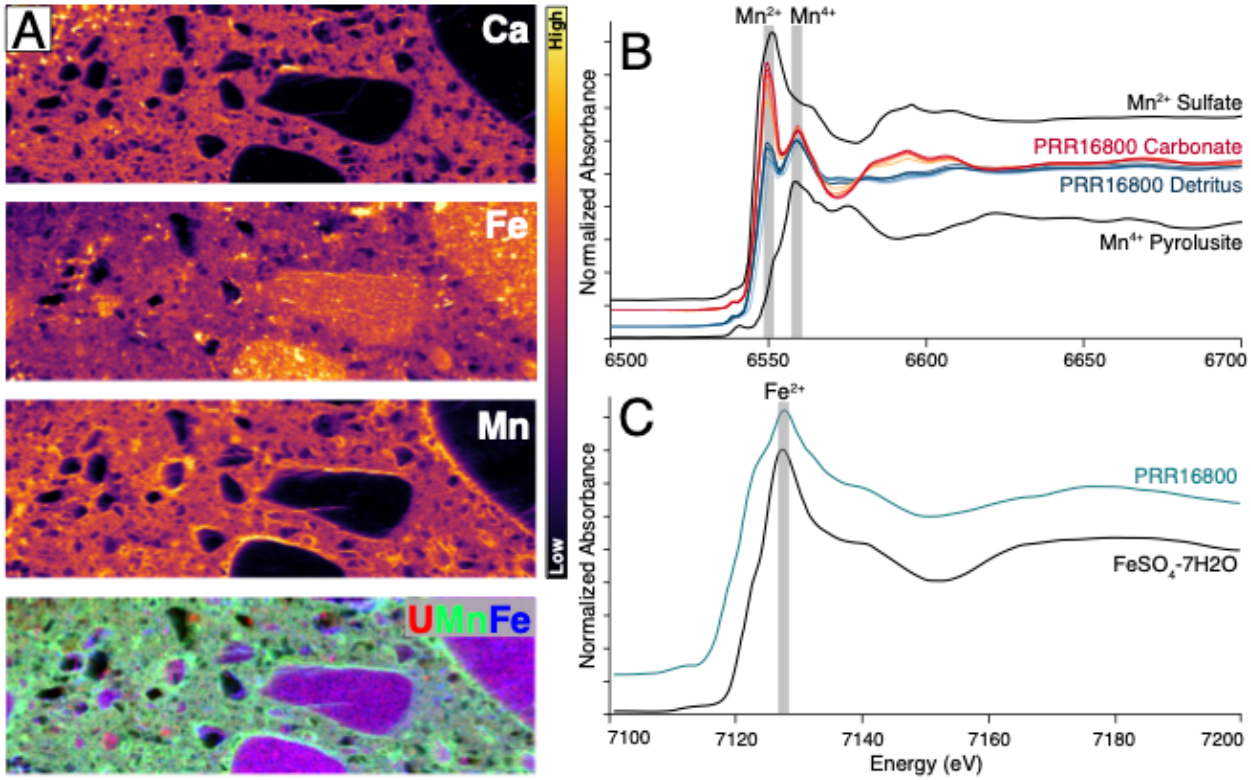

Figure 3: A: XRF maps of Ca, Fe, and Mn; RGB map of U, Mn, and Fe. Calcite and detrital minerals can be distinguished by areas of high and low abundance in the Ca map. B: Manganese K-edge μXANES. C: Iron K-edge μXANES. Sample spectra in B,C shown as colored curves; reference spectra shown as black curves.

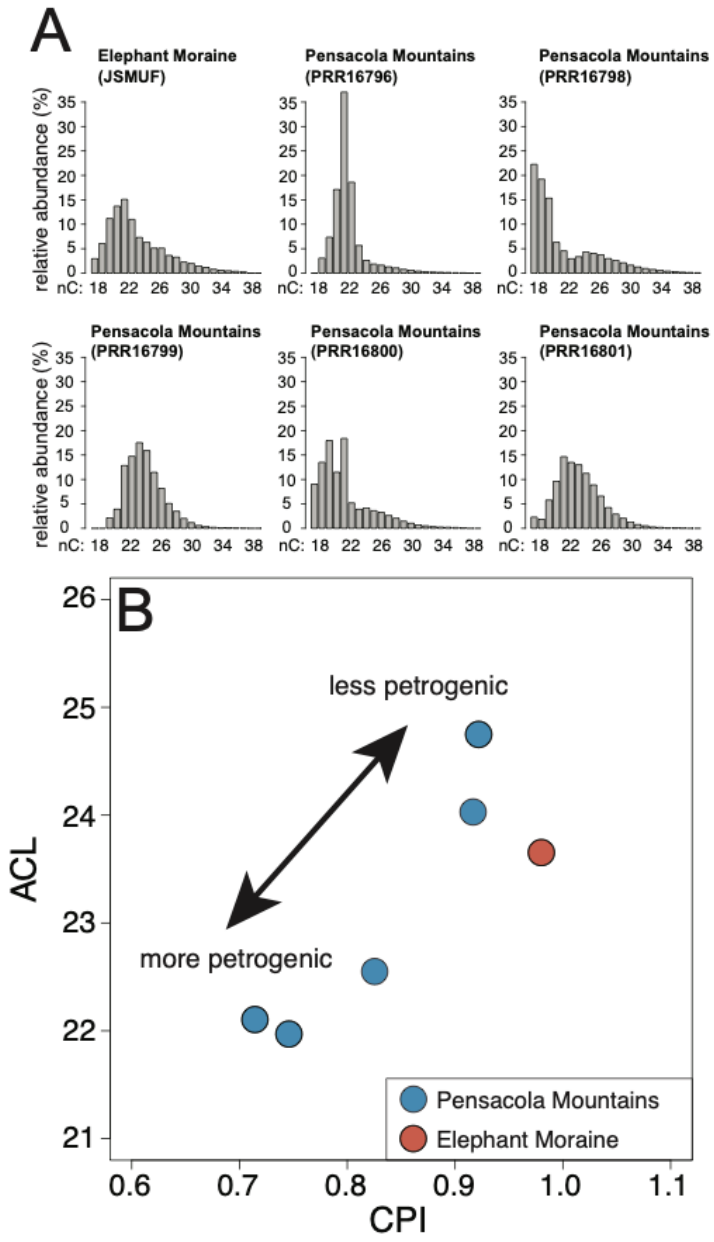

Figure 4: A: C_{18} to C_{40} *n*-alkane relative abundances. B: Correlation between *n*-alkane carbon preference index (an indicator of the degree of petrogenesis) and average chain length for each lipid biomarker analysis.

REFERENCES

Aitken, A.R.A. et al., 2023, Antarctic Sedimentary Basins and Their Influence on Ice-Sheet Dynamics: Reviews of Geophysics, v. 61, p. e2021RG000767, doi:10.1029/2021RG000767.

Beal, E.J., House, C.H., and Orphan, V.J., 2009, Manganese- and Iron-Dependent Marine Methane Oxidation: Science, v. 325, p. 184–187, doi:10.1126/science.1169984.

Bentley, M.J., Hein, A.S., Sugden, D.E., Whitehouse, P.L., Shanks, R., Xu, S., and Freeman, S.P.H.T., 2017, Deglacial history of the Pensacola Mountains, Antarctica from glacial geomorphology and cosmogenic nuclide surface exposure dating: Quaternary Science Reviews, v. 158, p. 58–76, doi:10.1016/j.quascirev.2016.09.028.

Blackburn, T., Edwards, G.H., Tulaczyk, S., Scudder, M., Piccione, G., Hallet, B., McLean, N., Zachos, J.C., Cheney, B., and Babbe, J.T., 2020, Ice retreat in Wilkes Basin of East Antarctica during a warm interglacial: Nature, v. 583, p. 554–559, doi:10.1038/s41586-020-2484-5.

Boetius, A., Ravenschlag, K., Schubert, C.J., Rickert, D., Widdel, F., Gieseke, A., Amann, R., Jørgensen, B.B., Witte, U., and Pfannkuche, O., 2000, A marine microbial consortium apparently mediating anaerobic oxidation of methane: Nature, v. 407, p. 623–626, doi:10.1038/35036572.

Boyd, E.S., Skidmore, M., Mitchell, A.C., Bakermans, C., and Peters, J.W., 2010, Methanogenesis in subglacial sediments: Environmental Microbiology Reports, v. 2, p. 685–692, doi:10.1111/j.1758-2229.2010.00162.x.

Bray, E.E., and Evans, E.D., 1961, Distribution of n-paraffins as a clue to recognition of source beds: Geochemica et Cosmochemica Acta, v. 22, p. 2–15.

Burns, R. et al., 2018, Direct isotopic evidence of biogenic methane production and efflux from beneath a temperate glacier: Scientific Reports, v. 8, p. 17118, doi:10.1038/s41598-018-35253-2.

Cassidy, W., Harvey, R., Schutt, J., Delisle, G., and Yanai, K., 1992, The meteorite collection sites of Antarctica: Meteoritics, v. 27, p. 490–525, doi:10.1111/j.1945-5100.1992.tb01073.x.

Christiansen, J.R., and Jørgensen, C.J., 2018, First observation of direct methane emission to the atmosphere from the subglacial domain of the Greenland Ice Sheet: Scientific Reports, v. 8, p. 2–7, doi:10.1038/s41598-018-35054-7.

Cochran, J.K., Landman, N.H., Jakubowicz, M., Brezina, J., Naujokaityte, J., Rashkova, A., Garb, M.P., and Larson, N.L., 2022, Geochemistry of Cold Hydrocarbon Seeps: An Overview, *in* Ancient Hydrocarbon Seeps, Cham, Springer International Publishing, Topics in Geobiology, v. 53, doi:10.1007/978-3-031-05623-9.

Crémière, A., Lepland, A., Chand, S., Sahy, D., Condon, D.J., Noble, S.R., Martma, T., Thorsnes, T., Sauer, S., and Brunstad, H., 2016, Timescales of methane seepage on the Norwegian margin following collapse of the Scandinavian Ice Sheet: Nature Communications, v. 7, p. 1–10, doi:10.1038/ncomms11509.

Davis, C.L. et al., 2023, Biogeochemical and historical drivers of microbial community composition and structure in sediments from Mercer Subglacial Lake, West Antarctica: ISME Communications, v. 3, p. 8, doi:10.1038/s43705-023-00216-w.

Dieser, M., Broemsen, E.L.J.E., Cameron, K.A., King, G.M., Achberger, A., Choquette, K., Hagedorn, B., Sletten, R., Junge, K., and Christner, B.C., 2014, Molecular and biogeochemical evidence for methane cycling beneath the western margin of the Greenland Ice Sheet: ISME Journal, v. 8, p. 2305–2316, doi:10.1038/ismej.2014.59.

Faure, G., 1990, Physical Description of the Elephant and Reckline Moraines, *in* Workshop on Antarctic Meteorite Standing Surfaces, p. 24–25.

Fretwell, P. et al., 2013, Bedmap2: Improved ice bed, surface and thickness datasets for Antarctica: Cryosphere, v. 7, p. 375–393, doi:10.5194/tc-7-375-2013.

Huggins, F.E., Huffman, G.P., Kosmack, D.A., and Lowenhaupt, D.E., 1988, MOSSBAUER DETECTION OF GOETHITE (~-FeOOH) IN COAL AND ITS POTENTIAL AS AN INDICATOR OF COAL OXIDATION:

Joye, S.B., 2020, The Geology and Biogeochemistry of Hydrocarbon Seeps: Annual Review of Earth and Planetary Sciences, v. 48, p. 205–231, doi:10.1146/annurev-earth-063016-020052.

Kvenvolden, K.A., and Rogers, B.W., 2005, Gaia's breath—global methane exhalations: Marine and Petroleum Geology, v. 22, p. 579–590, doi:10.1016/j.marpetgeo.2004.08.004.

Lamarche-Gagnon, G. et al., 2019, Greenland melt drives continuous export of methane from the ice-sheet bed: Nature, v. 565, p. 73–77, doi:10.1038/s41586-018-0800-0.

Lamb, A.L., Wilson, G.P., and Leng, M.J., 2006, A review of coastal palaeoclimate and relative sea-level reconstructions using δ13C and C/N ratios in organic material: Earth-Science Reviews, v. 75, p. 29–57, doi:10.1016/j.earscirev.2005.10.003.

Little, C.T.S., Birgel, D., Boyce, A.J., Crame, J.A., Francis, J.E., Kiel, S., Peckmann, J., Pirrie, D., Rollinson, G.K., and Witts, J.D., 2015, Late Cretaceous (Maastrichtian) shallow water hydrocarbon seeps from Snow Hill and Seymour Islands, James Ross Basin, Antarctica: Palaeogeography, Palaeoclimatology, Palaeoecology, v. 418, p. 213–228, doi:10.1016/j.palaeo.2014.11.020.

Machel, H.G., 2001, Bacterial and thermochemical sulfate reduction in diagenetic settings — old and new insights: Sedimentary Geology, v. 140, p. 143–175, doi:10.1016/S0037-0738(00)00176-7.

Michaud, A.B., Dore, J.E., Achberger, A.M., Christner, B.C., Mitchell, A.C., Skidmore, M.L., Vick-Majors, T.J., and Priscu, J.C., 2017, Microbial oxidation as a methane sink beneath the West Antarctic Ice Sheet: Nature Geoscience, v. 10, p. 582–586, doi:10.1038/NGEO2992.

Naehr, T.H., Eichhubl, P., Orphan, V.J., Hovland, M., Paull, C.K., Ussler, W., Lorenson, T.D., and Greene, H.G., 2007, Authigenic carbonate formation at hydrocarbon seeps in continental margin sediments: A comparative study: Deep Sea Research Part II: Topical Studies in Oceanography, v. 54, p. 1268–1291, doi:10.1016/j.dsr2.2007.04.010.

Paull, C.K., Chanton, J.P., Neumann, A.C., Coston, J.A., Martens, C.S., and Showers, W., 1992, Indicators of Methane-Derived Carbonates and Chemosynthetic Organic Carbon Deposits: Examples from the Florida Escarpment: PALAIOS, v. 7, p. 361–375, doi:10.2307/3514822.

Portnov, A., Vadakkepuliyambatta, S., Mienert, J., and Hubbard, A., 2016, Ice-sheet-driven methane storage and release in the Arctic: Nature Communications, v. 7, p. 10314, doi:10.1038/ncomms10314.

Preston, L.J., and Dartnell, L.R., 2014, Planetary habitability: lessons learned from terrestrial analogues: International Journal of Astrobiology, v. 13, p. 81–98, doi:10.1017/S1473550413000396.

Stibal, M. et al., 2012, Methanogenic potential of Arctic and Antarctic subglacial environments with contrasting organic carbon sources: Global Change Biology, v. 18, p. 3332–3345, doi:10.1111/j.1365-2486.2012.02763.x.

Sun, Y., Gong, S., Li, N., Peckmann, J., Jin, M., Roberts, H.H., Chen, D., and Feng, D., 2020, A new approach to discern the hydrocarbon sources (oil vs. methane) of authigenic carbonates forming at marine seeps: Marine and Petroleum Geology, v. 114, p. 104230, doi:10.1016/j.marpetgeo.2020.104230.

Wadham, J.L. et al., 2012, Potential methane reservoirs beneath Antarctica: Nature, v. 488, p. 633–637, doi:10.1038/nature11374.

Whiticar, M.J., 1999, Carbon and hydrogen isotope systematics of bacterial formation and oxidation of methane: Chemical Geology, v. 161, p. 291–314, doi:10.1016/S0009-2541(99)00092-3.

Wu, Y., Luo, S., Wang, D., Burns, S.J., Li, E., DeGroot, D.J., Yu, Y., and Zhang, G., 2021, Origin, growth, and characteristics of calcareous concretions in the varved sediments of a Glacial Lake: Engineering Geology, v. 287, p. 106112, doi:10.1016/j.enggeo.2021.106112.

Yang, K., Zhu, Z., Dong, Y., Chu, F., and Zhang, W., 2021, Evolution and diagenetic implications of framboids in the methane-related carbonates of the northern Okinawa Trough: Acta Oceanologica Sinica, v. 40, p. 114–124, doi:10.1007/s13131-021-1869-0.

Supplementary Information for:

Thermogenic Methane Production in Antarctic Subglacial Hydrocarbon Seeps

Gavin Piccione[1,2*], Jared E. Nirenberg[1,2], Joseph Novak[3], Abigale Hawthorn[4], Paul Northrup[5], Daniel E. Ibarra[1,2], Terrence Blackburn[4]

[1]Department of Earth, Environmental, and Planetary Sciences, Brown University, Providence, RI 02906, USA.
[2]Institute at Brown for Environment and Society, Brown University, Providence, RI 02906, USA.
[3]Ocean Sciences Department, University of California Santa Cruz, Santa Cruz, CA 95064, USA.
[4]Earth and Planetary Sciences, University of California Santa Cruz, Santa Cruz, CA 95064, USA.
5Department of Geosciences, Stony Brook University, Stony Brook, NY 11794, USA.

Corresponding author: Gavin Piccione (gavin_piccione@brown.edu)

This PDF includes:

Supplementary Materials Section 1

Figures S1 and S2

Supplementary References

Detailed Methods

Oxygen and carbon isotope ratios of carbonate ($\delta^{18}O$ and $\delta^{13}C$) were measured using a Thermo Scientific Kiel IV device and a MAT 253 isotope ratio mass spectrometer. Carbon isotopes of bulk organic matter within the subglacial precipitates ($\delta^{13}C_{org}$) were analyzed using a CE Instruments NC2500 elemental analyzer coupled to a Thermo Scientific DELTAplus XP isotope ratio mass spectrometer via a Thermo Scientific Conflo III. Both analyses were made at the UCSC Stable Isotope Laboratory following the procedures outlined in Piccione et al. (2022). Oxygen isotope compositions are reported as parent water values using the carbonate-water fractionation correction from Kim and O'Neil, (1997), and clumped isotope-constrained temperatures.

We measured carbonate clumped isotopes (Δ_{47}) at Brown University using an IBEX device and Thermo Scientific MAT 253+ isotope ratio mass spectrometer (Hodgin et al., 2024). Clumped isotope data were processed using the free software Easotope (John and Bowen, 2016). Instrument non-linearity was corrected with the pressure baseline correction methods (Bernasconi et al., 2013), and the Δ_{47} values were projected in the I-CDES inter-laboratory absolute reference frame (Bernasconi et al., 2021) based on frequently measured ETH 1, ETH 2, ETH 3, and ETH 4 standards. We use clumped isotope values to determine the carbonate formation temperatures, based on the calibration presented in (Anderson et al., 2021).

Uranium-series ($[^{234}U/^{238}U]_i$) isotope data were collected in the W.M. Keck Isotope laboratory at UCSC on an IsotopX X62 Thermal Ionization Mass Spectrometer following methods outlined in (Blackburn et al., 2020). Measurements were made on a single calcite aliquot, which was dissolved in 0.2 M nitric acid to avoid contamination from detrital minerals. We used the software IsoplotR to calculate and plot U-series isochrons and U-Th ages (Vermeesch, 2018).

Lipid biomarkers were processed and measured at Brown University. They were extracted at using a using a Dionex ASE 350 with a solvent mixture of 9:1 dichloromethane:methanol at 150˚C and 1500 psi with 3 static cycles of 5 minutes. The total lipid extracts were then separated using silica gel flash chromatography using 4 mL hexane, dichloromethane, and methanol as eluents. The hexane fraction was dried under N2, redissolved in 200 µL toluene, and analyzed using an Agilent 8890 gas chromatograph with a flame ionization detector. *n*-alkane peaks were assigned by comparing retention times with an *n*-alkane standard. The methanol fraction was dried under N_2, redissolved in 99:1 hexane:isopropanol, and filtered through a 0.45 µm polytetrafluoroethylene filter. C_{46} diol was added as an internal standard. GDGTs were analyzed using high performance liquid chromatography coupled with atmospheric pressure chemical ionization with selective ion monitoring (SIM) at m/z 1302, 1300, 1298, 1296, 1292, 1050, 1048, 1046, 1036, 1034, 1032, 1022, 1020, 1018, and 744. Two silica columns (Acquity UPLC BEH HILIC 1.7 µm, 2.1 by 150 mm) were run in series at 30˚C with a flow rate of 0.2 mL/min with mobile phases as in Hopmans et al., (2016). A laboratory standard was run before and after samples to ensure measurement quality.

X-Ray Florescence (XRF) maps and X-ray absorption near-edge structure (XANES) analyses were made at the National Synchrotron Light Source-II at Brookhaven National Laboratory using the 4-BM XFM beamline. For XRF maps, samples were mounted at 45° relative to the micro-focused incident beam with a spot size of 5 × 8 µm. Data were collected using on-the-fly scanning with a 125 ms dwell time using a four-element silicon-drift detector with incident energy tuned to 17.3 keV. Iron and manganese XANES were measured by step-scanning energy across their K absorption edges at 7.1 and 6.4 keV, respectively. We used the Athena software for normalization and analysis of XANES spectra (Ravel and Newville, 2005), and the Larch software for normalization and analysis of XRF maps (Newville, 2013).

SUPPLEMENTARY FIGURES

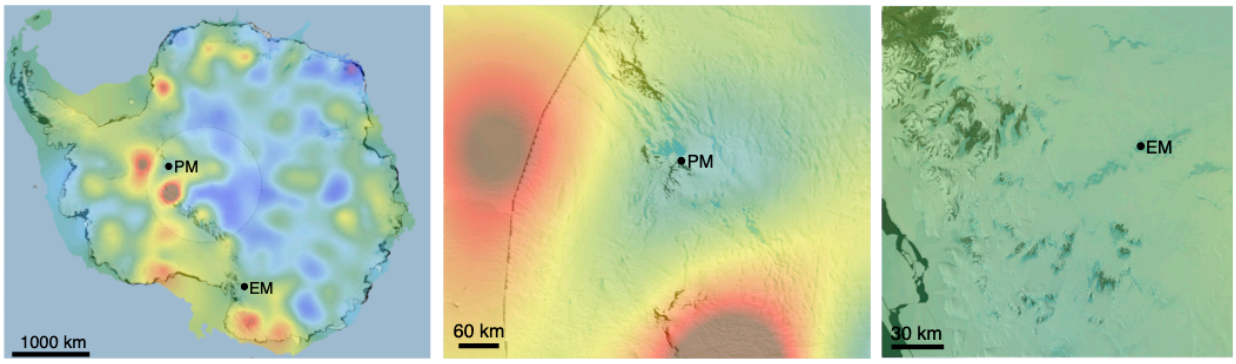

Supplementary Figure 1: Map of geothermal heat from the Elephant Moraine and Pensacola Mountains sites (Shapiro, 2004).

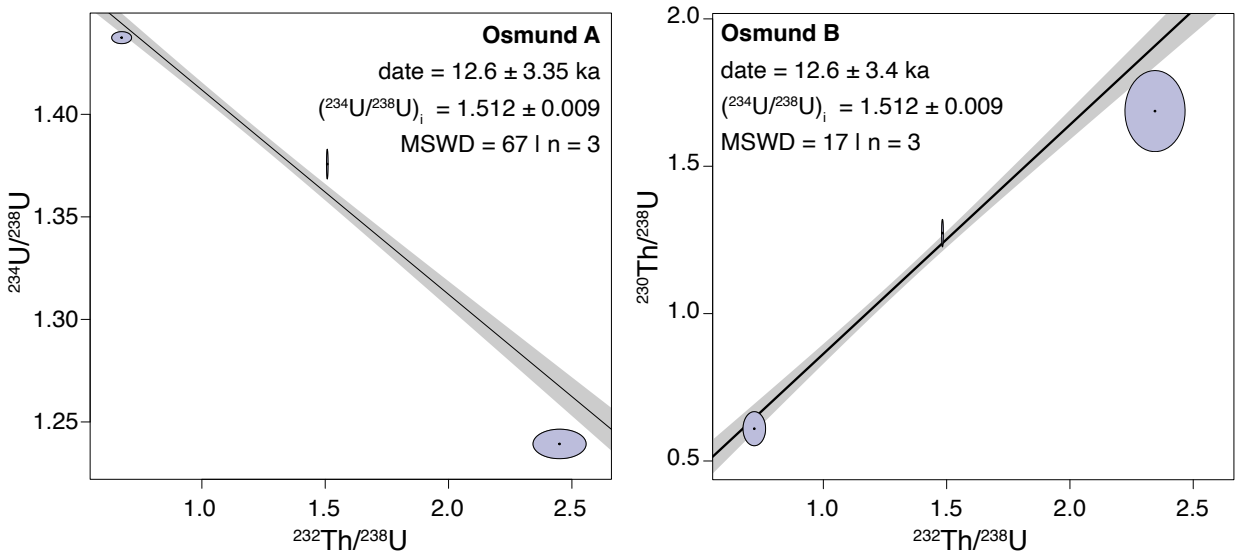

Supplementary Figure 2: U-series isochron from sample PRR54847 from the Pensacola Mountains.

REFERENCES

Anderson, N.T. et al., 2021, A Unified Clumped Isotope Thermometer Calibration (0.5–1,100°C) Using Carbonate-Based Standardization: Geophysical Research Letters, v. 48, p. 1–11, doi:10.1029/2020GL092069.

Bernasconi, S.M. et al., 2021, InterCarb: A Community Effort to Improve Interlaboratory Standardization of the Carbonate Clumped Isotope Thermometer Using Carbonate Standards: Geochemistry, Geophysics, Geosystems, v. 22, p. e2020GC009588, doi:10.1029/2020GC009588.

Bernasconi, S.M., Hu, B., Wacker, U., Fiebig, J., Breitenbach, S.F.M., and Rutz, T., 2013, Background effects on Faraday collectors in gas-source mass spectrometry and implications for clumped isotope measurements: Rapid Communications in Mass Spectrometry, v. 27, p. 603–612, doi:10.1002/rcm.6490.

Blackburn, T., Edwards, G.H., Tulaczyk, S., Scudder, M., Piccione, G., Hallet, B., McLean, N., Zachos, J.C., Cheney, B., and Babbe, J.T., 2020, Ice retreat in Wilkes Basin of East Antarctica during a warm interglacial: Nature, v. 583, p. 554–559, doi:10.1038/s41586-020-2484-5.

Hodgin, E.B., Swanson-Hysell, N.L., Kylander-Clark, A.R.C., Turner, A.C., Stolper, D.A., Ibarra, D.E., Schmitz, M.D., Zhang, Y., Fairchild, L.M., and Fuentes, A.J., 2024, One Billion Years of Stability in the North American Midcontinent Following Two-Stage Grenvillian Structural Inversion: Tectonics, v. 43, p. e2024TC008415, doi:10.1029/2024TC008415.

Hopmans, E.C., Schouten, S., and Sinninghe Damsté, J.S., 2016, The effect of improved chromatography on GDGT-based palaeoproxies: Organic Geochemistry, v. 93, p. 1–6, doi:10.1016/j.orggeochem.2015.12.006.

John, C.M., and Bowen, D., 2016, Community software for challenging isotope analysis: First applications of ‘Easotope’ to clumped isotopes: Rapid Communications in Mass Spectrometry, v. 30, p. 2285–2300, doi:10.1002/rcm.7720.

Kim, S.T., and O’Neil, J.R., 1997, Equilibrium and nonequilibrium oxygen isotope effects in synthetic carbonates: Geochimica et Cosmochimica Acta, v. 61, p. 3461–3475, doi:10.1016/S0016-7037(97)00169-5.

Newville, M., 2013, Larch: An Analysis Package for XAFS and Related Spectroscopies: Journal of Physics: Conference Series, v. 430, p. 012007, doi:10.1088/1742-6596/430/1/012007.

Ravel, B., and Newville, M., 2005, ATHENA , ARTEMIS , HEPHAESTUS : data analysis for X-ray absorption spectroscopy using IFEFFIT: Journal of Synchrotron Radiation, v. 12, p. 537–541, doi:10.1107/S0909049505012719.

458 Shapiro, N., 2004, Inferring surface heat flux distributions guided by a global seismic model:
459 particular application to Antarctica: Earth and Planetary Science Letters, v. 223, p. 213–
460 224, doi:10.1016/j.epsl.2004.04.011.

461 Vermeesch, P., 2018, IsoplotR: A free and open toolbox for geochronology: Geoscience Frontiers,
462 v. 9, p. 1479–1493, doi:10.1016/j.gsf.2018.04.001.